Article

Impact of Climate Change on the Glacier and Runoff of a Glacierized Basin in Harlik Mountain, Eastern Tianshan Mountains

Ping Zhou [1], Hui Zhang [1,2,*] and Zhongqin Li [1,2]

1   Tianshan Glaciological Station, State Key Laboratory of Cryospheric Science, Northwest Institute of Eco-Environment and Resources, Chinese Academy of Sciences, Lanzhou 730000, China; zhouping@lzb.ac.cn (P.Z.); lizq@lzb.ac.cn (Z.L.)

2   Altai Observation and Research Station of Cryospheric Science and Sustainable Development, State Key Laboratory of Cryospheric Science, Northwest Institute of Eco-Environment and Resources, Chinese Academy of Sciences, Lanzhou 730000, China

*   Correspondence: zhanghui@lzb.ac.cn; Tel.: +86-0931-4967383

Abstract: The impact of climate change on glaciers and the hydrological processes in the easternmost end of the eastern Tianshan Mountains has yet to be understood. This study investigated the glacier change (area, surface elevation and volume change) and analyzed the variation of the observed runoff series over the past four decades in the Yushugou Basin, Eastern Tianshan Mountains. The hydrological processes were also simulated through the HBV-light model to quantify the impact of climate change on the glacier and runoff. The results showed that the glacier area has decreased by 13% and the total volume has decreased by 0.018 km^3 over the past four decades. A significant increasing trend ($p < 0.01$) was detected for the annual runoff and monthly runoff (May to September; $p < 0.01$). The simulation results revealed that the Yushugou River was highly recharged by glacial runoff and a negative tendency was found for the glacier mass balance on the basin scale over the past 38 years. As a region with an extremely dry climate and the lowest precipitation in the Tianshan Mountains, the observation and simulation of glaciers is critical to the security assessment of local water resources.

Keywords: glacier change; runoff change; hydrological simulation; Yushugou Basin; Eastern Tianshan Mountains

1. Introduction

The Tianshan Mountains, known as the Water Tower of Central Asia, lie in the hinterland of Eurasia, which is one of the most developed mountain systems of modern glaciers in the world [1]. As an important water source in the middle of the "Silk Road Economic Belt", the Tianshan Mountains supply many large rivers in Central Asia, with an annual runoff of more than 100×10^8 m^3 [2]. Glaciers, functioning as freshwater reservoirs, are vital components of the local cycle [1,3–5], which provide considerable freshwater supply during dry periods for the densely populated, arid lowlands [1,6]. Glaciers store water in a solid form at different timescales, contribute to river runoff via meltwater, and play a role in regulating and maintaining the stability of river runoff for many years [7]. The Tianshan glaciers have repeatedly been shrinking and growing in the past few millennia [8,9], responding to warming and cooling phases [10]. Currently, there are 10,778 glaciers in the Tianshan Mountains of Central Asia, with a total area of about 13,566.6 km^2 (http://www.glims.org/RGI/index.html, accessed on 5 July 2020). Glacial meltwater in the summer period dominates the hydrological regime of the glacier-fed basin, providing a reliable source of water for irrigation, industry and hydropower, e.g., [1,11].

Over the past 54 years, the temperature in the Tianshan Mountains has warmed obviously, with a change rate of 0.3 °C·10 a^{-1}, which increased fastest in the Middle and East

Tianshan Mountains and increased slightly in the West Tianshan Mountains [5]. Meanwhile, annual precipitation exhibited an overall slight increasing trend, which increased obviously in the western and northern parts of the Tianshan Mountains and increased slightly in the Middle Tianshan Mountains. Precipitation on the northern and southern slopes of the Tianshan Mountains is strongly affected by the Indian summer monsoon (ISM) at the annual scale [12] while at an interannual scale, precipitation is mainly affected by the El Niño-Southern Oscillation (ENSO). Guan et al. [13] also reported that multi-decadal variability of the precipitation in winter was similar, with an East Atlantic-West Russia (EATL/WRUS) tele-connection pattern and the summer precipitation also impacted by the Scandinavia (SCAND) teleconnection pattern, the Silk Road pattern (SRP) and East Asia-Pacific teleconnection (EAP).

Affected by climatic change, most glaciers retreat and very few glaciers advance in the Tianshan Mountains [3,4,8,14], which affects the hydrological characteristics such as the quantity, seasonal distribution and temporal variability of the downstream rivers. Thus, it is necessary to quantify the impact of climate change on the variation of the glaciers and runoff under such a climatic background in the Tianshan Mountains.

Previous studies have been conducted to investigate the glacier recession [4,15–20] and its impact on hydrological processes, e.g., [1,6,21–30]. The hydrological model coupled with the glacier melt model is a common and useful tool to assess the impact of climate change on the glacier-fed streamflow regime. Zhao et al. [21] used the macro-scale hydrologic variable infiltration capacity model to simulate the runoff processes of the Kunma Like River catchment during the 1990 to 2007 period. Sun et al. [22] also simulated the hydrological processes of the glacier and snow melting through the HBV model in the Urumqi River source region in eastern Tianshan. Gao et al. [23] integrated a spatially distributed hydrological model (FLEXG) with Δh parameterization to estimate the runoff and historical glacier area variation of Urumqi Glacier No.1. Wang et al. [24] investigated the impact of precipitation and temperature changes on hydrological processes in the glacier-dominated catchment, Sary Djaz Kumaric River Basin. Zhang et al. [25] simulated the varying glacier area ratios in 24 headwater catchments and used them to explore the influence of various glaciers on runoff using the enhanced SWAT model. The glacier mass balance and hydrological processes of the Koxkar River Basin were modeled by Xu et al. [26] using the HBV model. Wang et al. [27] applied the modified HBV-D hydrological model to simulate hydrological processes at the headwater catchment of the Manas River Basin (MRB) in the Tianshan Mountains. Yang et al. [28] adopted a glacier dynamics model to simulate and predict hydrological changes in the headwater of the Urumqi River under three SSPs scenarios. Based on the different regional climate model outputs, Liu et al. [29] constructed a glacier-enhanced soil and water assessment tool and predicted the future runoff changes in the Jinghe River Basin. To quantify the future impact of climate change on hydrology, Khanal et al. [30] used the SPHY model to quantify the effects of climate change on the hydrological processes in 15 upstream rivers in High Mountain Asia.

The Yushugou Basin, located in the easternmost end of the eastern Tianshan Mountains (in China), has an extremely dry climate with the lowest precipitation in the Tianshan Mountains. Thus, glaciers and their meltwater are critical components of local water resources. Some observations and studies on glacier evolution (glacier mass balance, area and volume [20,31,32]) and hydrometeorology have been conducted over the past decades, although systematic research on hydrological process simulation is still lacking. Therefore, this study aimed to investigate the glacier change in the Yushugou Basin and analyze the temporal variation of the runoff series from 1979 to 2016, based on the observation data of the Yushugou Watershed Hydrological Observatory on the south slope of Harlik Mountain. We then simulated hydrological processes using the HBV-light model to explore the impact of climate change on hydrological processes, thus providing a scientific basis for rational utilization and optimal allocation of water resources in the downstream region.

2. Study Area

Yushugou Basin (43°02′–43°11′N; 93°57′–94°19′E) is located on the south slope of the Harlik Range, in the easternmost branch of Eastern Tianshan Mountains, close to Guxianghe Basin to the west and Miaoergou Basin to the east (Figure 1). Its runoff finally flows into the Hami Basin in the lower reaches. The climate is typical of a continental arid climate, with concentrated precipitation in the summer period and cold and dry winters, which is mainly influenced by the westerlies and Mongolia-Siberian high. Meteorological records of the Yushugou hydrological gauge (YHG) show that the mean annual temperature is approximately 5.9 °C and the annual precipitation is 143.9 mm, but about 79.6% of the precipitation occurs from May to September. Meanwhile, strong evaporation with an evaporation capacity and drought index of 1232.6 mm and 8.6 were detected [32]. The catchment area above the YHG was 314.67 km^2 and the altitude ranges from 1742.6 to 4643.4 m a.s.l. The zone above 4050 m a.s.l. is permanently covered by ice and snow. The highest and lowest altitude of the glacier terminus was 4758.6 and 3629 m a.s.l., respectively.
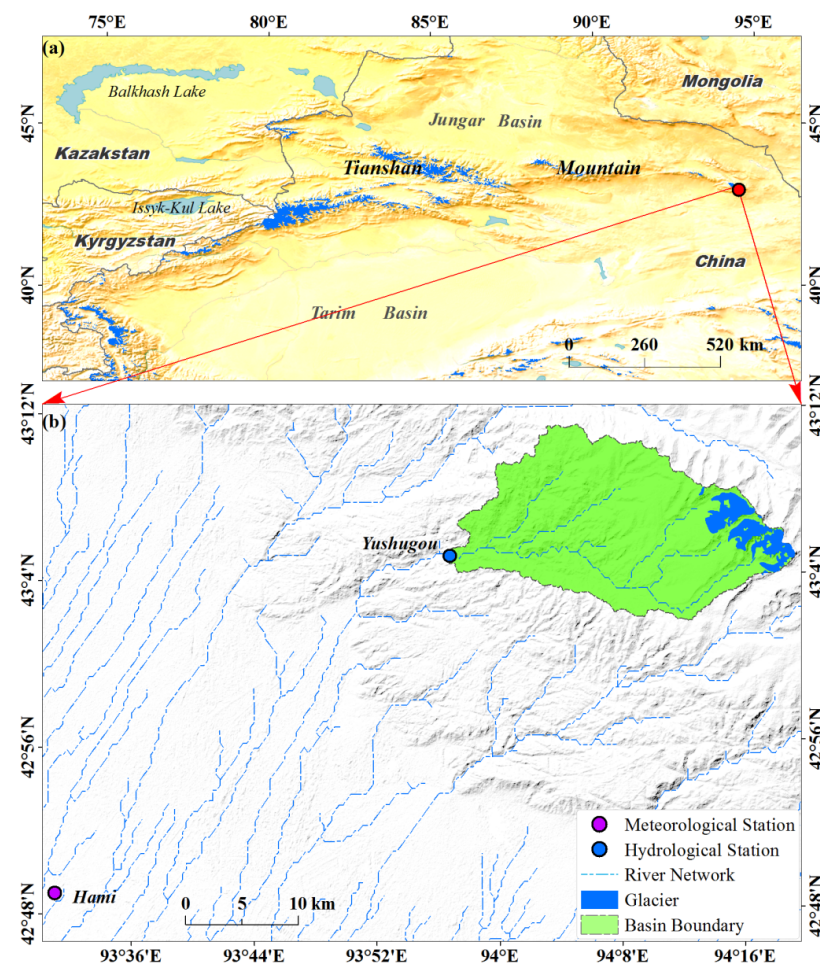

Figure 1. Map of the location of Yushugou Basin (**a**), sites of the hydrological station and meteorological station (**b**).

According to the Second Chinese Glacier Inventory, the area covered by glaciers in the basin was 20.02 km^2 and their volume ranged from 1.78 to 1.91 km^3 [33]. The total glacier area accounts for 6.4% of the total basin with an average glacier area of 2.53 km^2. An accelerated glacier mass balance was found with an average value of -0.26 ± 0.06 m w·e·a^{-1} from 1972 to 2015 [31]. Hydrological observation data from the YHG shows that the annual average runoff is approximately 0.53×10^8 m^3, with a C_v of 0.26 and a runoff depth of 142 mm. Runoff from May to September accounts for about 87.7% of the total runoff while runoff from the other months is mainly supplied by groundwater discharge [32]. The

downstream region of the basin is surrounded by the vast barren sands of the Gobi; hence, glacier/snow meltwater is a critical source of water to the local hydrological cycle.

3. Data and Method

3.1. Data

Monthly runoff (1979–2016) and meteorological data (temperature and precipitation; 2003–2010) from YHG were used in this study. YHG (43.08°N; 93.95°E; 1670 m a.s.l.) is the only hydrological gauge to collect hydrological data in the basin. Due to the lack of long-series and high-resolution meteorological observation data in the alpine region, temperature and precipitation data from Hami National Meteorological Station (HAM) were chosen to quantify local climate change. The distance between HAM and the hydrological station is only 45 km, and the data was provided by the China Meteorological Administration (http://data.cma.cn/, accessed on 1 May 2021). Given the high spatial variation of precipitation in the alpine region, grid dataset meteorological data for precipitation (with a spatial resolution of $0.5° \times 0.5°$) released by the National Meteorological Information Center of the China Meteorological Administration was also selected, which has wide applications in the Tianshan Mountains [34,35]. Meanwhile, SRTM DEM was applied to extract the altitudinal information of the basin and glacier, with a spatial resolution of 90 m (https://earthexplorer.usgs.gov/, accessed on 1 June 2021). Topographic maps (with a scale of 1:50,000) in July 1972 provided by the Chinese Military Geodetic Service and Landsat TM 5/OLI 8 remote sensing images were used to extract the glacial boundaries, obtained from USGS (Table 1). Glacier surface elevation changes (1972–2015) in Harlik Mountain were quantified through the topographic maps, SRTM X-band radar data and ASTER images [31]. The result was used to extract the surface elevation changes of the glaciers in the study region.

Table 1. Remote sensing data used in this study.

Path	ID	Date	Resolution (m)
138/30	LT51380301989235BJC00	1989/08/23	30
138/30	LT51380301999231BJC00	1999/08/19	30
138/30	LT51380302008224BJC01	2008/08/11	30
138/30	LC81380302016214LGN02	2016/08/01	30

3.2. Methods

To recognize concurrent trends in the meteorological-hydrology series, the widely used Mann–Kendall test [36,37] was applied to detect the annual hydro-meteorological time series. The null hypothesis assumes no rising or falling trend in the time series. Mathematically, the test statistic is as follows:

$$S = \sum_{i=1}^{n-1} \sum_{j=i+1}^{n} \text{sign}(x_j - x_i)$$

where x_i and x_j are the corresponding values at times i and j, and n is the length of the data sets.

The Z statistic is an index for evaluating the significance of trend statistics, which can be described by:

$$Z = \begin{cases} \frac{S-1}{\sqrt{\frac{n(n-1)(2n+5)}{18}}} & \text{if} \quad S > 0 \\ 0 & \text{if} \quad S = 0 \\ \frac{S+1}{\sqrt{\frac{n(n-1)(2n+5)}{18}}} & \text{if} \quad S < 0 \end{cases}$$

when Z is $-1.96 \leq Z \leq 1.96$, the null hypothesis is accepted, which indicates that the tendency of the sequence is not obvious. The trend is significant at 95% confidence if

$|Z| > 1.96$, and at 99% confidence if $|Z| > 2.58$. A positive value of Z suggests a growth tendency while a negative value reflects a declining tendency.

Suppose the trend is linear and there is an estimated median slope between all possible pairs (x_i and x_j). The magnitude of the trend can be evaluated by:

$$b = \text{Median}\left(\frac{x_j - x_i}{j - i}\right) \quad \forall j > i \quad i = 1, 2, \ldots, n - 1$$
$$j = 2, \ldots, n$$

where $1 < i < j < n$, positive b reflects an increasing trend, and negative b shows a decreasing trend. The tipping point of the runoff series was captured through the Mann–Kendall abrupt change test, which was verified by the sliding t-test and Yamamoto test. Meanwhile, morlet wavelet analysis was also applied to reveal the periodic change in the runoff series.

The classical ratio threshold method was used to initially extract the glacier surface extent based on the Landsat TM/OLI images. The band ratio for Landsat 5 and Landsat 8 was TM3/TM5 and TM4/TM6, respectively. Considering the uncertainty from snow, debris and shade, the boundary was corrected through manual visual interpretation. Uncertainty from the topographic map and remote sensing image interpretation is mainly influenced by the image resolution and co-registration error, which were calculated by the following formulae [38,39]:

$$U_T = \sqrt{\sum \lambda^2} + \sqrt{\sum \varepsilon^2}$$
$$U_A = 2U_T \sqrt{\sum \lambda^2} + \sqrt{\sum \varepsilon^2}$$

where U_T and U_A are the uncertainty of the glacier area and glacier length, respectively; and λ and ε are the uncertainty from image resolution and co-registration separately, respectively. According to the above analysis, the uncertainty in boundary delineation was calculated as ± 0.003 km^2 using the Landsat images and ± 0.0025 km^2 using topographic maps.

To generate the forcing dataset of the hydrological model, the observed monthly meteorological data (temperature and precipitation) of YHG was compared to that of the Hami station and the grid dataset. The results show that there was a significant correlation for the temperature data between HM and YHG ($r = 0.99$, $p < 0.01$) and for the precipitation data between YHG and the grid dataset ($r = 0.86$, $p < 0.01$). Thereby, we generated the daily temperature series (1972–2016) of YHG through the statistical downscaling method [34,40] based on the temperature data of HAM and YHG. The daily precipitation series of the grid dataset was corrected through the ratio method on a monthly scale [41]. The ratios of monthly precipitation were obtained by a comparison of the total monthly precipitation amounts of the grid data and YHG separately. As is shown in Figure 2, the corrected temperature data and precipitation data significantly correlate with the observed data in HAM and the grid data, respectively, with a low root mean square error (*RMSE*).
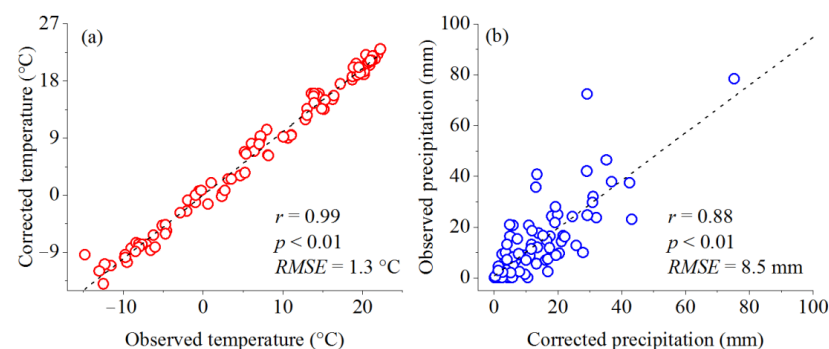

Figure 2. Comparison of the observed temperature data at YHG versus the corrected temperature series at HM (**a**) and the observed precipitation data at YHG versus the corrected precipitation of the grid data (**b**) from January 2003 to December 2010.

To assess the response of the hydrological process to climate change, a semi-distributed conceptual rainfall-runoff model—the HBV-light model—was applied in this study, which divides the basin into different altitude zones and vegetation zones according to altitude and simulates the runoff process of multiple sub-basins through different time steps [42]. Meanwhile, the glacier/snow module based on the classical temperature index model was coupled to depict the ice/snow ablation process in the basin. Up to now, the model has wide applications in the simulation of hydrological processes in cold alpine regions [43–45]:

$$P - E - Q = \frac{d}{dt}(SP + SM + UZ + LZ)$$

where P, E and Q are precipitation, evaporation and discharge, respectively. SP and SM represent snowpack and soil moisture, and UZ and LZ are the upper and lower groundwater zones. The model was forced by daily air temperature, daily precipitation and monthly potential evapotranspiration as input data to simulate daily runoff. The model is divided into five modules: the glacier module, snow module, soil module, response function and routine module [42].

When the temperature (T) is above the threshold temperature (TT), the ablation of snow starts. In contrast, when the temperature (T) is below the threshold temperature (TT), the accumulation is solid-type precipitation and the meltwater retained in the snowpack would refreeze. Snowmelt ($Melt_{snow}$) was calculated by a temperature-index method, which is equal to the degree-day factor of snow ($CFMAX$) multiplied by the temperature difference ($T - TT$):

$$Melt_{snow} = CFMAX \times (T - TT)$$

The ablation of the glacier was also calculated using the temperature-index model, in which the degree-day factor was equal to CFMAX multiplied by the correction factor ($CF_{glacier}$). Accumulation was also equal to the sum of solid precipitation on the glacier surface. The relationship between the glacial water content and outflow (Q_g) varies over time:

$$Melt_{ice} = \mathrm{CF}_{glacier} \times CFMAX \times (T - TT)$$

$$Q_g = \left(KGmin + dKG \times e^{-AG \times SWE}\right) \times S$$

where $KGmin$ is the minimum outflow coefficient; dKG is the maximum minus minimum outflow coefficient; AG is the calibration parameter; SWE is the water equivalent of the snowpack on top of the glacier; and S is the liquid water content of the glacier.

Water filling of the soil box is split into rainfall (P) and snowmelt. Groundwater recharge depends on the relationship between the water content of the soil box (SM) and its largest value (FC):

$$\frac{recharge}{P} = \left(\frac{SM}{FC}\right)^{BETA}$$

$BETA$ is the parameter that determines the relative contribution to runoff from rain or snowmelt:

$$E_{act} = E_{pot} \times min\left(\frac{SM}{FC \times LP}, 1\right)$$

where E_{act} is actual evapotranspiration; E_{pot} is potential evapotranspiration; and LP is the soil moisture value above which E_{act} reaches E_{pot}. If SM/FC is greater than LP, actual evaporation from the soil box equals evaporation. While SM/FC is less than LP, actual evaporation reduces linearly.

Meanwhile, E_{pot} is calculated by the method proposed by [46], which was estimated by:

$$E_{pot} = 0.0023 R_s (T + 17.78)(\mathrm{T}_{max} - \mathrm{T}_{min})^{0.5}$$

where T is the mean daily temperature; T_{max} and T_{min} are the minimum temperature and maximum temperature separately; and R_s is solar radiation, which was calculated

according to the latitude and time. The three linear outflow equations are used to calculate runoff from the groundwater boxes, which depend on whether the storage in the soil upper zone is above the threshold parameter. Finally, the simulated runoff is obtained by a triangle weighting function defined by the parameter MAXBAS [42].

To obtain the optimal parameter combination, the model parameters were calibrated and determined by an automatic procedure (Monte Carlo calibration). In this study, the Nash–Sutcliffe efficiency coefficient (R_{eff}) and the coefficient of determination (r^2) were used to evaluate the model performance:

$$R_{eff} = 1 - \frac{\sum (Q_{sim}(t) - Q_{obs}(t))^2}{\sum (Q_{obs}(t) - \overline{Q_{obs}})^2}$$

$$r^2 = \frac{\left(\sum \left(Q_{obs(t)} - \overline{Q_{obs(t)}} \right) \left(Q_{sim(t)} - \overline{Q_{sim(t)}} \right) \right)^2}{\sum \left(Q_{obs(t)} - \overline{Q_{obs(t)}} \right)^2 \sum \left(Q_{sim(t)} - \overline{Q_{sim(t)}} \right)^2}$$

where $Q_{obs}(t)$ and $Q_{sim}(t)$ are the observed and simulated runoff, respectively. $\overline{Q_{obs(t)}}$ and $\overline{Q_{sim(t)}}$ are the average of the observed and simulated runoff, respectively, during the study period.

4. Results

4.1. Glacier Area and Surface Elevation Change

The glacier area of the Yushugou Basin decreased by 13% (3.57 km^2) from 1972 to 2016. The glacier area reduced by 1.95, 0.58, 0.55 and 0.49 km^2 during the periods of 1972–1989, 1989–2000, 2000–2007 and 2007–2016, with a relative change rate of 8%, 3%, 3% and 2%, respectively. One glacier disappeared over the past 44 years.

As is shown in Figure 3, the surface elevation of the glaciers in the Yushugou Basin decreased significantly over the past 43 years. For the whole basin, the mean elevation change was estimated by -0.12 m·a^{-1} from 1972 to 2000 and -0.42 m·a^{-1} from 2000 to 2015, which results in an mass loss rate of 0.10 and 0.37 m w·e·a^{-1}, respectively. The total volume has decreased by 0.018 km^3 over the past 43 years. It can be seen that mass loss accelerated significantly after 2000 in comparison to the period of 1972–2000.
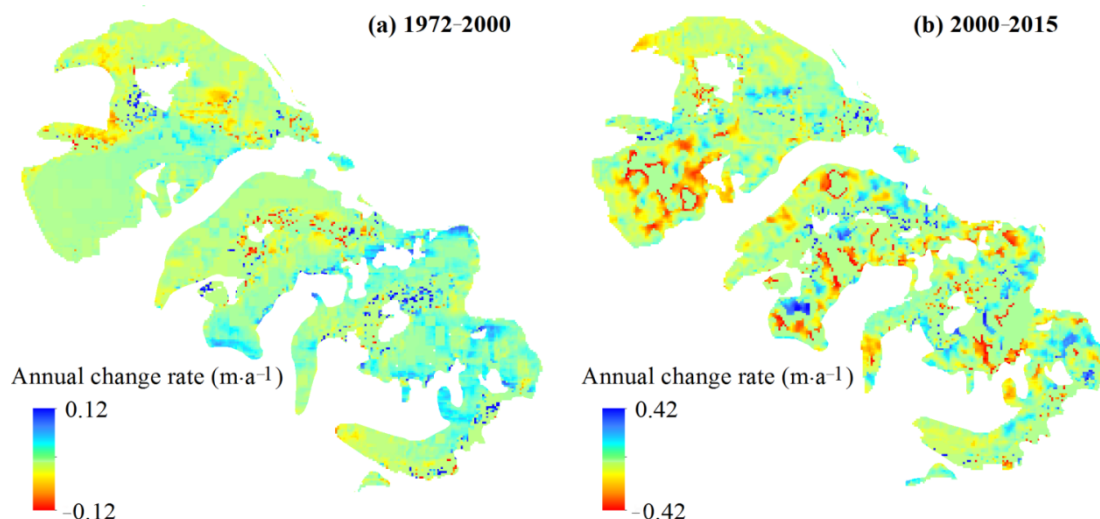

Figure 3. Surface elevation changes of the glaciers in the Yushugou Basin from 1972 to 2000 and 2000 to 2015.

4.2. Variation of Annual Runoff and Monthly Runoff

As is shown in Figure 4, the annual runoff of the Yushugou Basin exhibits a significant increasing trend ($p < 0.01$), with a change rate of 0.047 $\times$ 10^8 m^3·10 a^{-1} and an average

value of 0.53×10^8 m^3. The maximum value (0.79×10^8 m^3) occurs in 2010 while the minimum value appears in 1985. The accumulated difference curve shows that three periods were distinguished for the annual runoff series. The runoff decreased sharply in period I (1979–1989), entered into a stable phase in period II (1990–1998) and increased significantly in period III (1999–2016). The average value of period III is obviously higher than that of the former two periods.
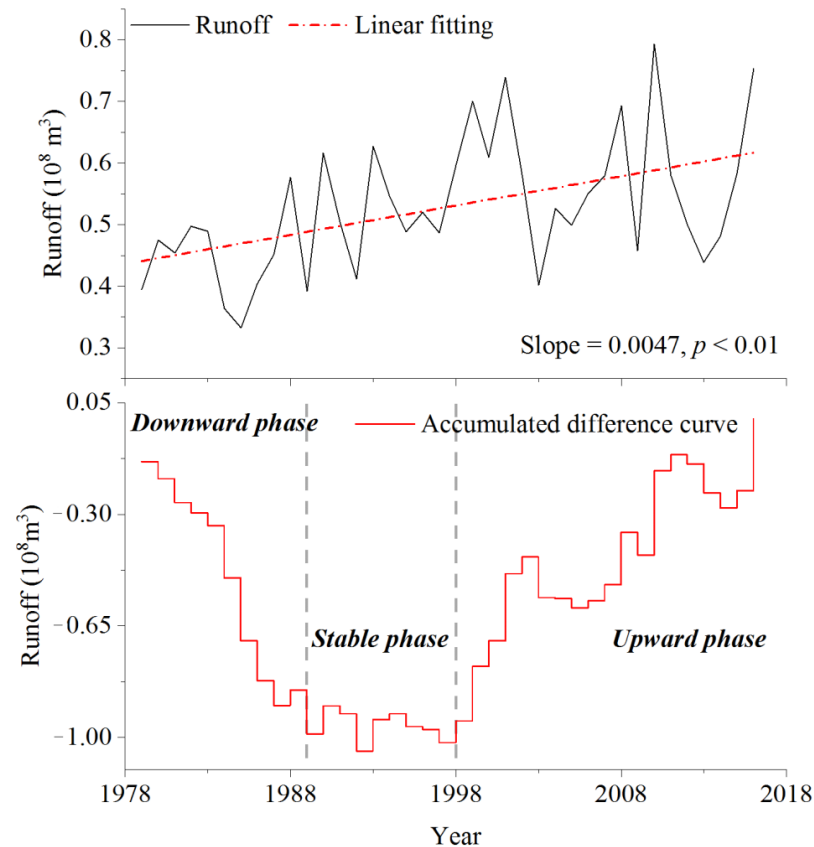
Figure 4. Variation of the annual runoff series in the Yushugou Basin from 1979 to 2016.

Moreover, the mutation test analysis shows that the tipping point of the annual runoff series emerged around 1990 under the significance test level of 0.05 (Figure 5). After this point, annual runoff turned to an upward trend and increased significantly. The results of wavelet analysis show that there are 3–6 years and 6–20 years of periodical fluctuation between high flow years and low flow years in the processes of runoff change. In comparison, the periodic fluctuation of the latter is more obvious.
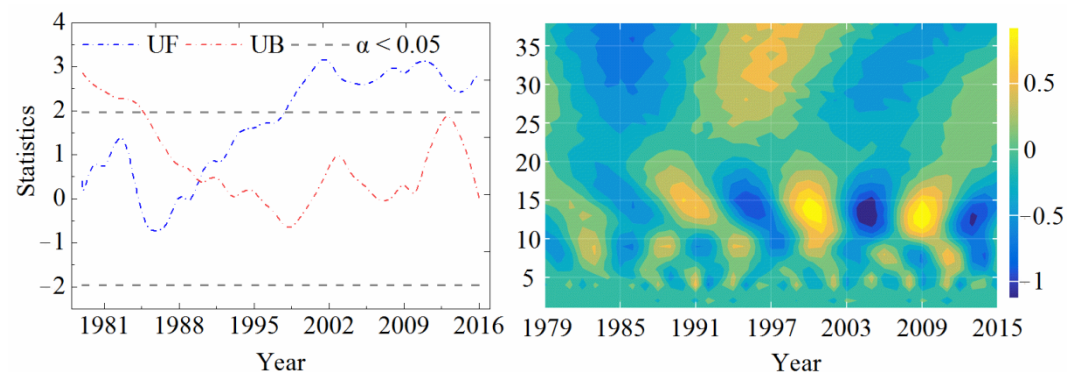
Figure 5. Mutation test analysis and wavelet analysis of the runoff series in the Yushugou Basin from 1979 to 2016.

In total, 86% of the runoff occurs from May to September, with a typical "single peak" distribution. However, differences in the magnitude and interannual variation for the monthly flow still exist. The mean monthly flow ranges from 0.20 to 5.70 $m^3 \cdot s^{-1}$, among which the maximum value occurs in July (5.70 $m^3 \cdot s^{-1}$), followed by August (4.55 $m^3 \cdot s^{-1}$), June (3.85 $m^3 \cdot s^{-1}$), May (1.93 $m^3 \cdot s^{-1}$) and September (1.60 $m^3 \cdot s^{-1}$). For the remaining months, both are lower than 1 $m^3 \cdot s^{-1}$, with the minimum value in February. Over the past 38 years, the monthly flow in January, May and October to December showed a slight downward trend while that from May to September exhibited a significant increasing trend ($p < 0.01$). The increasing magnitude for the flow in July (0.750 $m^3 \cdot s^{-1} \cdot 10 \ a^{-1}$) is largest, followed by August (0.525 $m^3 \cdot s^{-1} \cdot 10 \ a^{-1}$), June (0.375 $m^3 \cdot s^{-1} \cdot 10 \ a^{-1}$) and September (0.194 $m^3 \cdot s^{-1} \cdot 10 \ a^{-1}$) (Figure 6). For February, March and April, these values are relatively lower. In general, the increment in the flow in the summer period (June to August) is the main contributor to the increment in the annual value.
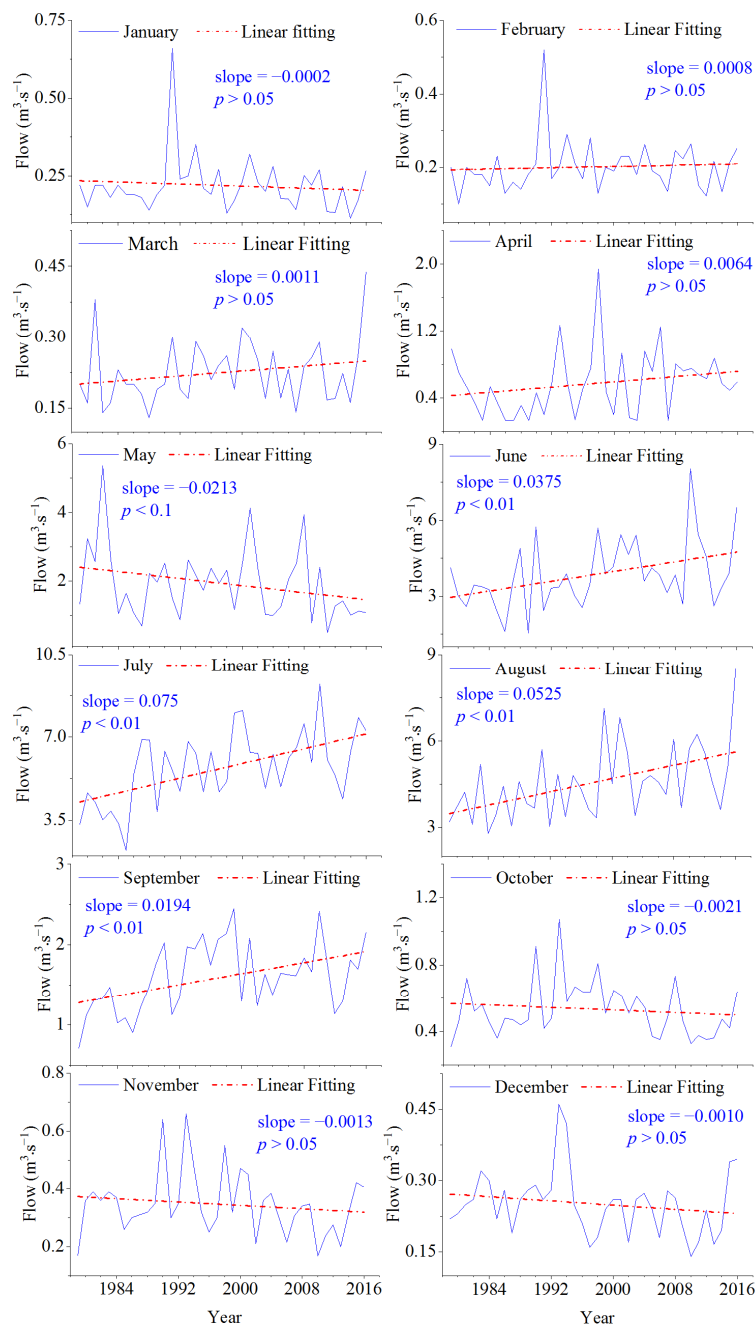

Figure 6. Variation of the monthly flow in the Yushugou Basin from 1979 to 2016.

4.3. Performance Evaluation of the Hydrological Model

The basin is divided into 15 elevation zones (including glacial and non-glacial zones, which feature bare and sparse grass < 15%) with an elevation interval of 207.20 m. The HBV model was forced by the corrected daily temperature, daily precipitation and calculated monthly average potential evaporation. The model contains 24 parameters distributed in 5 modules (Table 2). The initial range of the parameters was set according to the existing observations and related references. Given the observation uncertainty of the critical parameters (precipitation gradient and temperature gradient), their initial range was adjusted to within $\pm 20\%$.

Table 2. Optimized parameter set of the HBV model.

Parameter	Description	Prior Range	Value1	Value2	References
PCALT	precipitation gradient (%/100 m)	$12.6 \pm 20\%$	10.01	10.01	[32]
TCALT	temperature gradient (°C/100 m)	$0.55 \pm 20\%$	0.61	0.61	[47]
TT	threshold temperature to split snowfall and rainfall (°C)	−2.5–2.5	−0.41	0.18	[48]
CFMAX	degree-day factor of snow $(mm/(°C \cdot d)^{-1})$	2–6	3.1	3.15	[49]
SP	seasonal variability in CFMAX (−)	0–1	0.31	0.33	-
SFCF	snowfall correction factor (−)	0–1	0.55	0.43	[45]
CFR	refreezing coefficient (−)	0.05–0.2	0.02	0.02	[45]
CWH	water holding capacity (−)	0–0.2	0.3	0.29	[48]
FC	maximum soil moisture storage (mm)	50–500	140	160	[50]
LP	soil moisture value above which AET reaches PET (mm)	0.3–1	0.53	0.33	[50]
BETA	the parameter that determines the relative contribution to runoff from rain or snowmelt (−)	1–6	0.72	0.79	[50]
$CF_{Glacier}$	glacier correction factor (−)	1.2–1.6	1.3	1.5	[51]
CF_{Slope}	slope correction factor (−)	1–2	0.82	0.87	[45]
KSI	snow to Ice conversion factor (d^{-1})	0–0.1	0.02		[21]
KG_{min}	minimum outflow coefficient t (d^{-1})	0.01–0.4	0.01		[51]
dKG	maximum minus minimum outflow coefficient (d^{-1})	0.01–0.5	0.05		[51]
AG	calibration parameter (mm^{-1})	0–1	0.02		*
PERC	threshold parameter (mm/d)	0–6	5		[48]
UZL	threshold parameter (mm)	0–50	13		[50]
K0	storage (or recession) coefficient 0 (d^{-1})	0.1–0.5	0.02		[50]
K1	storage (or recession) coefficient 1 (d^{-1})	0.05–0.3	0.002		[50]
K2	storage (or recession) coefficient 2 (d^{-1})	0.001–0.1	0.003		[50]
MAXBAS	length of triangular weighting function (d)	1–5	2		[48]
Cet	potential evaporation correction factor	0–1	0.001		*

* indicates the default valid range of model values. Value1 and Value2 are the parameters of glacier zone 1 and non-glacier zone 2, respectively.

All YHG hydrological data were used to calibrate the model parameters and validate the simulation result, referring to the previous study [52]. The optimal parameter combination and the comparison between the simulated and observed values are displayed in Table 2 and Figure 7. There is good consistency between the simulated flow and the measured flow from 1979 to 2016, except for a few years. The *Reff* and R^2 for the model were 0.77 and 0.91, respectively, which substantiates the model's robustness in this study.

4.4. Variation of the Modeled Runoff Components Series

The simulated results show that the contribution ratio to total runoff for the glacial runoff, rainfall runoff and snowmelt runoff was 63.4%, 25.3% and 11.3%, respectively. As shown in Figure 8, the simulated rainfall runoff shows an insignificant increasing trend ($p > 0.05$) over the past 38 years, with a change rate of 0.01×10^8 m$^3 \cdot 10$ a^{-1}. The simulated snowmelt runoff also exhibited a significant increasing trend ($p < 0.01$), with an increasing rate of 0.009×10^8 m$^3 \cdot 10$ a^{-1}. The simulated glacial runoff also showed a significant upward trend ($p < 0.01$) with a change rate of 0.025×10^8 m$^3 \cdot 10$ a^{-1}. The significant low-value period occurred from 1991 to 1997 and the glacial runoff increased significantly after 1997. The simulated glacier mass balance exhibited a decreasing trend from 1979 to

2016, with a decline rate of -8.16 mm w·e·10 a^{-1}. The glacier mass balance decreased significantly after 1997, and the accumulated glacier mass balance was -4.80 m w·e· over the past 38 years, which is basically consistent with the results of Wan et al. [31].
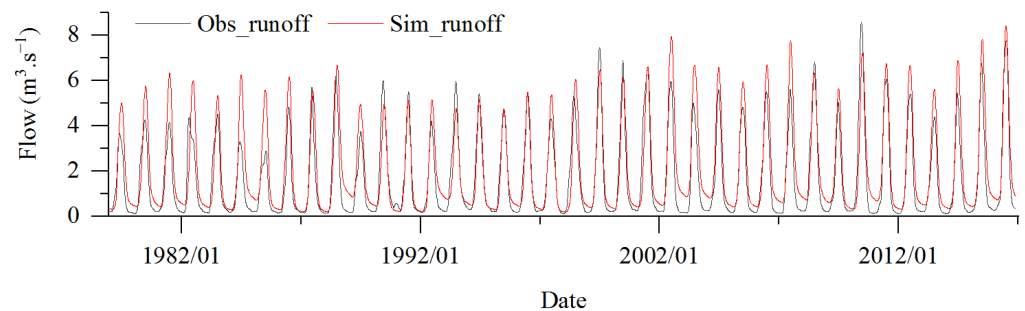

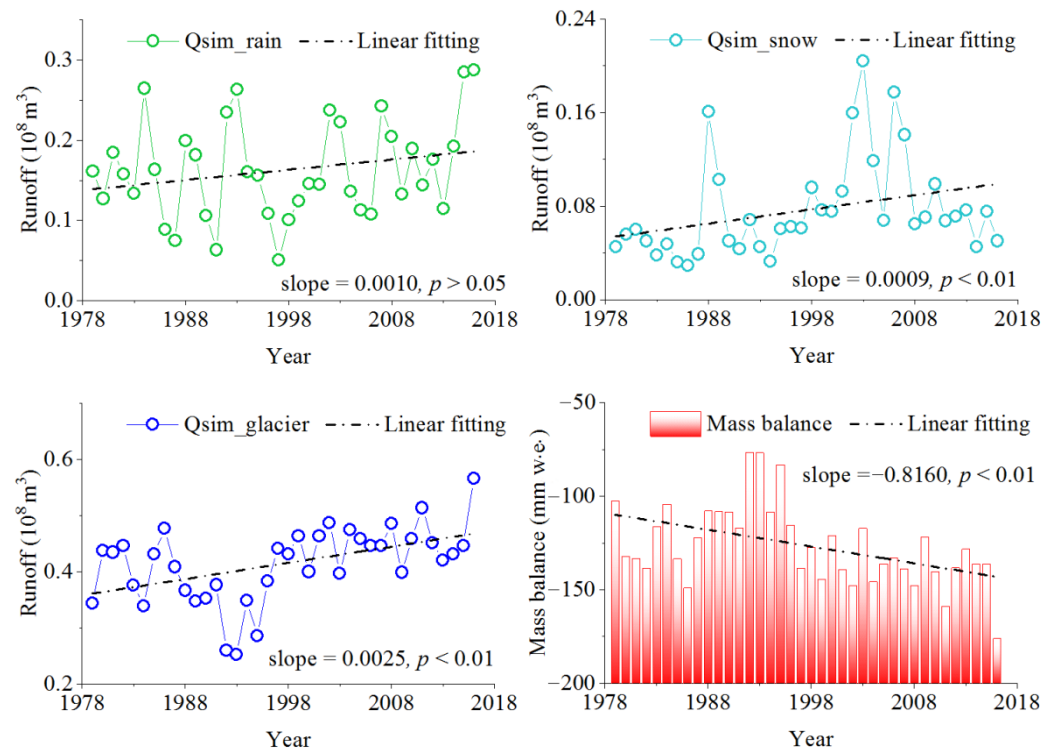**Figure 7.** Comparison of the observed monthly flow and simulated monthly flow of YHG from 1979 to 2016.

Figure 8. Variation of the simulated rainfall runoff (Qsim_rain), simulated snowmelt runoff (Qsim_snow), simulated glacial runoff (Qsim_glacier) and glacier mass balance from 1979 to 2016.

5. Discussion

The glacier area of the Yushugou Basin decreased by 13% and the surface elevation thinned significantly over the past 43 years. A significant increasing trend ($p < 0.01$) was also detected for the annual runoff of the Yushugou Basin, with a change rate of 0.047×10^8 m^3·10 a^{-1}. The tipping point of the annual runoff emerged around 1990 ($p < 0.05$), and the runoff increased significantly after that. Monthly flow from May to September exhibited a significant increasing trend ($p < 0.01$), and a slight increasing/decreasing trend was found in the remaining months from 1979 to 2016. The modeled results showed that the contribution ratio of the three components (Qsim_glacier, Qsim_rain and Qsim_snow) to the total runoff was 63.4%, 25.3% and 11.3%, respectively. Wang et al. (2017) found that the total runoff recharged 54.9% of the glacier meltwater through isotopes and hydrochemistry, a result that is lower than ours. The simulated snowmelt runoff and glacial runoff both exhibited a significant increasing trend ($p < 0.01$), and an insignificant trend was detected for the simulated rainfall runoff

over the past 38 years. The glacier mass balance of the Yushugou Basin had a negative tendency, and the accumulated glacier mass balance was −4.80 m w·e·.

Over the past 38 years, the annual temperature showed an increased trend at a rate of 0.18 °C·10 a^{-1} based on the model forcing data. As shown in Figure 9, periodic changes in temperature are evident and increased more significantly after 1997. Precipitation also exhibited an increasing tendency, with an increasing rate of 8.96 mm·10 a^{-1}. The mean annual precipitation during the period of 1998–2016 (161.33 mm) is obviously larger than that of the period of 1972–1997 (128.70 mm).
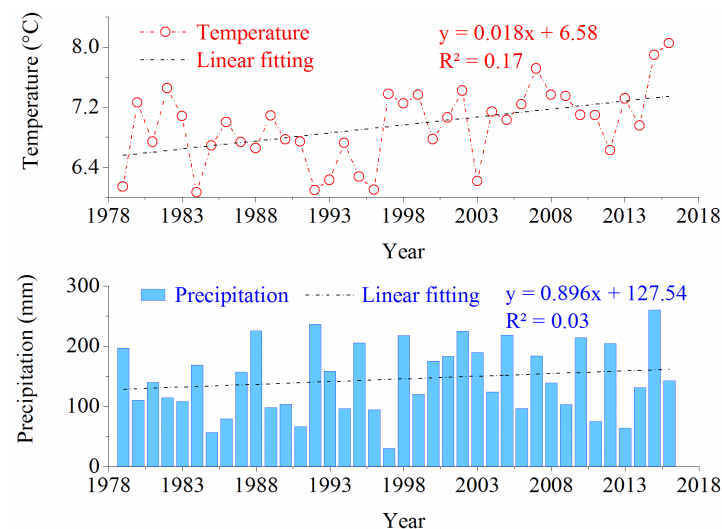
Figure 9. Variation of the annual temperature and precipitation from 1979 to 2016.

To further explore the relationship between the corrected meteorological data (temperature and precipitation) and runoff, we compared the accumulated difference curves of the temperature, precipitation, total runoff, Qsim_rain, Qsim_glacier and Qsim_snow (Figure 10). The results showed that the runoff in period I (1979 to 1989) showed a downward trend, affected by the decrease in temperature and precipitation. Secondly, the total runoff entered the lowest period in period II (1990 to 1997), affected by the decrease in precipitation and glacial runoff due to the decrease in air temperature. A higher glacier mass balance also emerged in this period. In period III (1998 to 2016), the temperature showed a significant upward trend while the precipitation increased sharply from 1998 to 2004 and was generally stable after 2004. Thus, the snowmelt runoff and glacial runoff increased significantly under the influence of increased temperature, which eventually led to a significant increase in the total runoff. In addition, the evaporation of the Yushugou Basin was higher, with an annual value of 1232.6 mm [32], which may also weaken the yield of rainfall runoff.

To explore the sensitivity of the runoff to climatic fluctuation, the temperature and precipitation were adjusted under the four designed climatic conditions: adjusting the temperature change to within ±10%, keeping precipitation unchanged, and adjusting the precipitation to within ±10%, keeping the temperature unchanged. The results revealed that the total runoff is more sensitive to changes in temperature in comparison to changes in precipitation. When temperature increases/decreases by 10%, the total runoff increases/decreases by around 30% (Figure 11). In addition, Qsim_glacier increases/decreases significantly by around 47% under the same climatic conditions while Qsim_rain and Qsim_snow are significantly sensitive to changes in precipitation in comparison with temperature fluctuations. Given the high contribution ratio of the glacial runoff to total runoff, the increment in the total runoff is mainly controlled by the temperature rise, followed by the increase in precipitation. In addition, simulations of the hydrological processes and hydrometeorological observation in the YHG Basin are still needed.
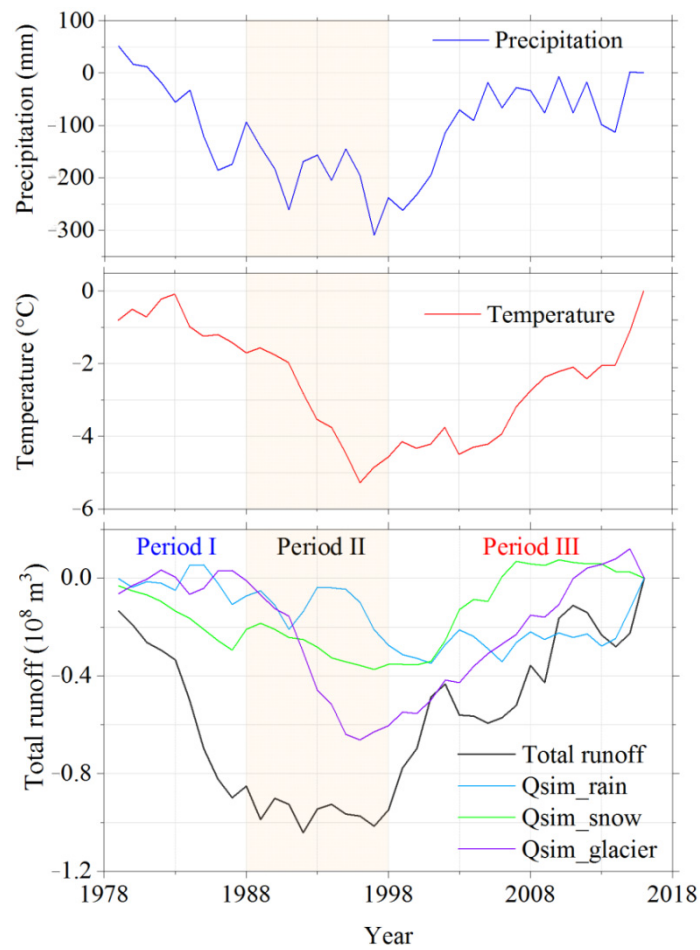
Figure 10. Comparison of the accumulated curves for temperature, precipitation, total runoff, Qsim_rain, Qsim_glacier and Qsim_snow. Period II is indicated by the light orange.
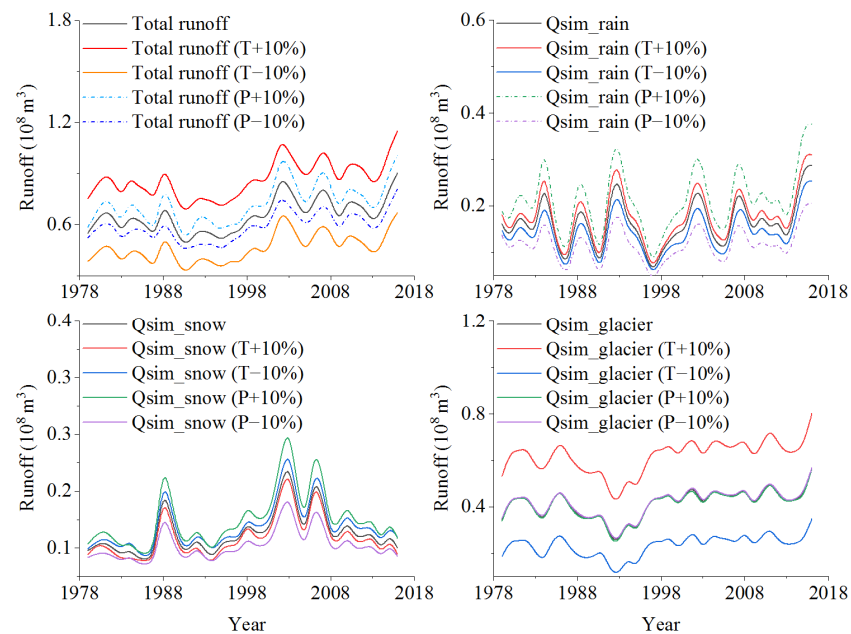

Figure 11. Sensitivity analysis for the total runoff, Qsim_rain, Qsim_glacier and Qsim_snow under the four climatic conditions.

6. Conclusions

In this study, we investigated variations in the glacier area, surface elevation, and runoff changes at annual and monthly scales in the Yushugou Basin over the past four decades. The hydrological process was simulated through the HBV-light model. The results showed that the glacier area in the Yushugou Basin decreased by 13% from 1972 to 2016, and the total volume decreased by 0.018 km^3 from 1972 to 2015. The annual runoff of the Yushugou Basin exhibited a significant increasing trend ($p < 0.01$), and the runoff from May to September also exhibited a significant increasing trend ($p < 0.01$) from 1979 to 2016. The contribution ratio of the simulated glacial runoff, rainfall runoff and snowmelt runoff to the total runoff were 63.4%, 25.3% and 11.3%, respectively. A negative tendency was found for the glacier mass balance on the basin scale over the past 38 years. It can be seen that glacial runoff and snowmelt runoff almost dominate the runoff changes of the Yushugou Basin, especially for glacial runoff. As a region with an extremely dry climate and the lowest precipitation in the Tianshan Mountains, observation and simulation of glaciers in the study region is critical to the security assessment of regional water resources under the background of climate change. Model sensitivity analysis combined with climate change analysis showed that the impact of temperature fluctuation on runoff is higher than that of precipitation. The increment in the annual runoff after 1998 can be primarily attributed to the temperature rise. Considering the shortage of meteorological observation data and the limitations of the model in hydrological process analysis, more comprehensive hydro-meteorological observations in mountainous areas and sophisticated simulation are still needed.

Author Contributions: Conceptualization, H.Z.; Data curation, P.Z.; Formal analysis, H.Z.; Funding acquisition, Z.L.; Investigation, P.Z.; Methodology, H.Z. All authors have read and agreed to the published version of the manuscript.

Data Availability Statement: Data available on request from the authors.

Conflicts of Interest: The authors declare no conflict of interest.

References

1. Sorg, A.; Bolch, T.; Stoffel, M.; Solomina, O.; Beniston, M. Climate change impacts on glaciers and runoff in Tien Shan (Central Asia). *Nat. Clim. Change* **2012**, *2*, 725–731. [CrossRef]
2. Chen, Y.; Li, Z.; Fang, G. Changes of key hydrological elements and research progress of water cycle in the Tianshan Mountains, Central Asia. *Arid. Land Geogr.* **2022**, *45*, 1–8. (In Chinese)
3. Immerzeel, W.W.; van Beek, L.P.H.; Bierkens, M.F.P. Climate Change Will Affect the Asian Water Towers. *Science* **2010**, *328*, 1382–1385. [CrossRef] [PubMed]
4. Farinotti, D.; Longuevergne, L.; Moholdt, G.; Duethmann, D.; Molg, T.; Bolch, T.; Vorogushyn, S.; Guntner, A. Substantial glacier mass loss in the Tien Shan over the past 50 years. *Nat. Geosci.* **2015**, *8*, 716–722. [CrossRef]
5. Chen, Y.N.; Li, W.H.; Deng, H.J.; Fang, G.H.; Li, Z. Changes in Central Asia's Water Tower: Past, Present and Future. *Sci. Rep.* **2016**, *6*, 35458. [CrossRef]
6. Hagg, W.; Braun, L.N.; Weber, M.; Becht, M. Runoff modelling in glacierized Central Asian catchments for present-day and future climate. *Nord. Hydrol.* **2006**, *37*, 93–105. [CrossRef]
7. Jansson, P.; Hock, R.; Schneider, T. The concept of glacier storage: A review. *J. Hydrol.* **2003**, *282*, 116–129. [CrossRef]
8. Li, Y.; Lu, X.; Li, Y. A Review on the Little Ice Age and Factors to Glacier Changes in the Tian Shan, Central Asia. In *Glacier Evolution in a Changing World*; Godone, D., Ed.; IntechOpen: London, UK, 2017; pp. 38–54.
9. Savoskul, O.S.; Solomina, O.N. Late-Holocene glacier variations in the frontal and inner ranges of the Tian Shan, central Asia. *Holocene* **1996**, *6*, 25–35. [CrossRef]
10. Zhang, Y.; Kong, Z.C.; Yan, S.; Yang, Z.J.; Ni, J. "Medieval Warm Period" on the northern slope of central Tianshan Mountains, Xinjiang, NW China. *Geophys. Res. Lett.* **2009**, *36*, L11702. [CrossRef]

11. Vyazov, L.A.; Ershova, E.G.; Ponomarenko, E.V.; Gajewski, K.; Blinnikov, M.S.; Sitdikov, A.G. Ancient Society of the Lake Balkhash Basin. In *Socio-Environmental Dynamics along the Historical Silk Road*; Springer: Cham, Switzerland, 2019; pp. 381–382.

12. An, L.X.; Hao, Y.H.; Yeh, T.C.J.; Zhang, B.J. Annual to multidecadal climate modes linking precipitation of the northern and southern slopes of the Tianshan Mts. *Theor. Appl. Clim.* **2020**, *140*, 453–465. [CrossRef]

13. Guan, X.F.; Yao, J.Q.; Schneider, C. Variability of the precipitation over the Tianshan Mountains, Central Asia. Part II: Multi-decadal precipitation trends and their association with atmospheric circulation in both the winter and summer seasons. *Int. J. Climatol.* **2022**, *42*, 139–156. [CrossRef]

14. Zhou, S.G.; Yao, X.J.; Zhang, D.H.; Zhang, Y.; Liu, S.Y.; Min, Y.F. Remote Sensing Monitoring of Advancing and Surging Glaciers in the Tien Shan, 1990–2019. *Remote Sens.* **2021**, *13*, 1973. [CrossRef]

15. Li, K.M.; Li, Z.Q.; Gao, W.Y.; Wang, L. Recent glacial retreat and its effect on water resources in eastern Xinjiang. *Chin. Sci. Bull.* **2011**, *56*, 3596–3604. [CrossRef]

16. Bolch, T. Climate change and glacier retreat in northern Tien Shan (Kazakhstan/Kyrgyzstan) using remote sensing data. *Glob. Planet Change* **2007**, *56*, 1–12. [CrossRef]

17. Narama, C.; Kaab, A.; Duishonakunov, M.; Abdrakhmatov, K. Spatial variability of recent glacier area changes in the Tien Shan Mountains, Central Asia, using Corona (similar to 1970), Landsat (similar to 2000), and ALOS (similar to 2007) satellite data. *Glob. Planet Change* **2010**, *71*, 42–54. [CrossRef]

18. Li, Z.Q.; Li, H.L.; Chen, Y.N. Mechanisms and Simulation of Accelerated Shrinkage of Continental Glaciers: A Case Study of Urumqi Glacier No. 1 in Eastern Tianshan, Central Asia. *J. Earth Sci.* **2011**, *22*, 423–430. [CrossRef]

19. Pieczonka, T.; Bolch, T. Region-wide glacier mass budgets and area changes for the Central Tien Shan between similar to 1975 and 1999 using Hexagon KH-9 imagery. *Global Planet Change* **2015**, *128*, 1–13. [CrossRef]

20. Wang, Y.T.; Hou, S.G.; Liu, Y.P. Glacier changes in the Karlik Shan, eastern Tien Shan, during 1971/72-2001/02. *Ann. Glaciol.* **2009**, *50*, 39–45. [CrossRef]

21. Zhao, Q.D.; Zhang, S.Q.; Ding, Y.J.; Wang, J.; Han, H.D.; Xu, J.L.; Zhao, C.C.; Guo, W.Q.; Shangguan, D.H. Modeling Hydrologic Response to Climate Change and Shrinking Glaciers in the Highly Glacierized Kunma Like River Catchment, Central Tian Shan. *J. Hydrometeorol.* **2015**, *16*, 2383–2402. [CrossRef]

22. Sun, M.P.; Li, Z.Q.; Yao, X.J.; Zhang, M.J.; Jin, S. Modeling the hydrological response to climate change in a glacierized high mountain region, northwest China. *J. Glaciol.* **2015**, *61*, 127–136. [CrossRef]

23. Gao, H.K.; Li, H.; Duan, Z.; Ren, Z.; Meng, X.Y.; Pan, X.C. Modelling glacier variation and its impact on water resource in the Urumqi Glacier No. 1 in Central Asia. *Sci. Total Environ.* **2018**, *644*, 1160–1170. [CrossRef] [PubMed]

24. Wang, X.L.; Luo, Y.; Sun, L.; Zhang, Y.Q. Assessing the effects of precipitation and temperature changes on hydrological processes in a glacier-dominated catchment. *Hydrol. Process* **2015**, *29*, 4830–4845. [CrossRef]

25. Zhang, Y.Q.; Luo, Y.; Sun, L.; Liu, S.Y.; Chen, X.; Wang, X.L. Using glacier area ratio to quantify effects of melt water on runoff. *J. Hydrol.* **2016**, *538*, 269–277. [CrossRef]

26. Xu, M.; Han, H.D.; Kang, S.C. Modeling Glacier Mass Balance and Runoff in the Koxkar River Basin on the South Slope of the Tianshan Mountains, China, from 1959 to 2009. *Water* **2020**, *12*, 582. [CrossRef]

27. Wang, X.Y.; Yang, T.; Xu, C.Y.; Xiong, L.H.; Shi, P.F.; Li, Z.Y. The response of runoff components and glacier mass balance to climate change for a glaciated high-mountainous catchment in the Tianshan Mountains. *Nat. Hazards* **2020**, *104*, 1239–1258. [CrossRef]

28. Yang, M.; Li, Z.Q.; Anjum, M.N.; Kayastha, R.; Kayastha, R.B.; Rai, M.; Zhang, X.; Xu, C.H. Projection of Streamflow Changes Under CMIP6 Scenarios in the Urumqi River Head Watershed, Tianshan Mountain, China. *Front. Earth Sci.* **2022**, *10*, 857854. [CrossRef]

29. Liu, J.; Long, A.H.; Deng, X.Y.; Yin, Z.L.; Deng, M.J.; An, Q.; Gu, X.C.; Li, S.Y.; Liu, G.H. The Impact of Climate Change on Hydrological Processes of the Glacierized Watershed and Projections. *Remote Sens.* **2022**, *14*, 1314. [CrossRef]

30. Khanal, S.; Lutz, A.F.; Kraaijenbrink, P.D.A.; van den Hurk, B.; Yao, T.; Immerzeel, W.W. Variable 21st Century Climate Change Response for Rivers in High Mountain Asia at Seasonal to Decadal Time Scales. *Water Resour. Res.* **2021**, *57*, e2020WR029266. [CrossRef]

31. Wan, Z.J.; Wang, Y.T.; Hou, S.G.; Huai, B.J.; Liu, Q. A doubling of glacier mass loss in the Karlik Range, easternmost Tien Shan, between the periods 1972–2000 and 2000–2015. *J. Glaciol.* **2021**, *67*, 1–12. [CrossRef]

32. Luo, G.; AI, L.; Qi, X.M.; Xu, L.C.; Li, B. Hydrological Characteristics of the Yushugou Valley. *Bimon. Xinjiang Meteorol.* **2002**, *25*, 19–37. (In Chinese)

33. Guo, W.Q.; Liu, S.Y.; Xu, L.; Wu, L.Z.; Shangguan, D.H.; Yao, X.J.; Wei, J.F.; Bao, W.J.; Yu, P.C.; Liu, Q.; et al. The second Chinese glacier inventory: Data, methods and results. *J. Glaciol.* **2015**, *61*, 357–372. [CrossRef]

34. Zhang, H.; Li, Z.Q.; Zhou, P.; Zhu, X.F.; Wang, L. Mass-balance observations and reconstruction for Haxilegen Glacier No.51, eastern Tien Shan, from 1999 to 2015. *J. Glaciol.* **2018**, *64*, 689–699. [CrossRef]

35. Zhu, X.F.; Zhang, M.J.; Wang, S.J.; Qiang, F.; Zeng, T.; Ren, Z.G.; Dong, L. Comparison of monthly precipitation derived from high-resolution gridded datasets in arid Xinjiang, central Asia. *Quatern Int.* **2015**, *358*, 160–170. [CrossRef]

36. Kendall, M.G. Rank Correlation Methods. *Br. J. Psychol.* **1990**, *25*, 86–91. [CrossRef]

37. Mann, H.B. Nonparametric Tests against Trend. *Econometrica* **1945**, *13*, 245–259. [CrossRef]

38. Hall, D.K.; Bayr, K.J.; Schoner, W.; Bindschadler, R.A.; Chien, J.Y.L. Consideration of the errors inherent in mapping historical glacier positions in Austria from the ground and space (1893–2001). *Remote Sens. Environ.* **2003**, *86*, 566–577. [CrossRef]

39. Silverio, W.; Jaquet, J.M. Glacial cover mapping (1987–1996) of the Cordillera Blanca (Peru) using satellite imagery. *Remote Sens. Environ.* **2005**, *95*, 342–350. [CrossRef]

40. Fujita, K.; Nuimura, T. Spatially heterogeneous wastage of Himalayan glaciers. *Proc. Natl. Acad. Sci. USA* **2011**, *108*, 14011–14014. [CrossRef]

41. Yang, W.; Yao, T.D.; Guo, X.F.; Zhu, M.L.; Li, S.H.; Kattel, D.B. Mass balance of a maritime glacier on the southeast Tibetan Plateau and its climatic sensitivity. *J. Geophys. Res. Atmos.* **2013**, *118*, 9579–9594. [CrossRef]

42. Seibert, J.; Vis, M.J.P. Teaching hydrological modeling with a user-friendly catchment-runoff-model software package. *Hydrol. Earth Syst. Sci.* **2012**, *16*, 3315–3325. [CrossRef]

43. Gadeke, A.; Holzel, H.; Koch, H.; Pohle, I.; Grunewald, U. Analysis of uncertainties in the hydrological response of a model-based climate change impact assessment in a subcatchment of the Spree River, Germany. *Hydrol. Process* **2014**, *28*, 3978–3998. [CrossRef]

44. Pomeon, T.; Jackisch, D.; Diekkruger, B. Evaluating the performance of remotely sensed and reanalysed precipitation data over West Africa using HBV light. *J. Hydrol.* **2017**, *547*, 222–235. [CrossRef]

45. Ali, A.F.; Xiao, C.D.; Zhang, X.P.; Adnan, M.; Iqbal, M.; Khan, G. Projection of future streamflow of the Hunza River Basin, Karakoram Range (Pakistan) using HBV hydrological model. *J. Mt. Sci.* **2018**, *15*, 2218–2235. [CrossRef]

46. Hargreaves, H.G.; Samani, A.Z. Reference Crop Evapotranspiration from Temperature. *Appl. Eng. Agric.* **1985**, *1*, 96–99. [CrossRef]

47. Liu, C.; Ding, L. A primary calculation of temperature and precipitation in Tianshan Mountains, China. *J. Glaciol. Geocryol.* **1988**, *10*, 151–159. (In Chinese)

48. Seibert, J. Estimation of parameter uncertainty in the HBV model. *Nord. Hydrol.* **1997**, *28*, 247–262. [CrossRef]

49. Wu, L.H.; Li, H.L.; Wang, L. Application of a Degree-Day Model for Determination of Mass Balance of Urumqi Glacier No. 1, Eastern Tianshan, China. *J. Earth Sci.* **2011**, *22*, 470–481. [CrossRef]

50. Seibert, J. Multi-criteria calibration of a conceptual runoff model using a genetic algorithm. *Hydrol. Earth Syst. Sci.* **2000**, *4*, 215–224. [CrossRef]

51. Zhang, X.P.; Qin, X.; Xu, C.H.; Liu, Y.S. Simulation of Runoff and Glacier Mass Balance and Sensitivity Analysis in a Glacierized Basin, North-Eastern Qinhai-Tibetan Plateau, China. *Water* **2018**, *10*, 1259. [CrossRef]

52. Shen, H.; Tolson, B.A.; Mai, J. Time to Update the Split-Sample Approach in Hydrological Model Calibration. *Water Resour. Res.* **2022**, *58*, e2021WR031523. [CrossRef]